CHEMICAL ABUNDANCE OF CO AND HCO+ IN NGC 253

Ishika Gobin
Instructor: Dr. Jeff Mangum

University of Virginia
Department of Astronomy

May 9, 2025

This thesis is submitted in partial completion of the BS Astronomy-Physics Major.

Preprint typeset using LaTeX style emulateapj v. 12/16/11

CHEMICAL ABUNDANCE OF CO AND HCO+ IN NGC 253

I. Gobin[1], J.Mangum[2], E. Behrens[2]

ABSTRACT

We present a study of the molecular gas distribution in the nearby starburst galaxy NGC 253 using observations from the Atacama Large Millimeter/submillimeter Array (ALMA) as part of the ALMA Comprehensive High-Resolution Extragalactic Molecular Inventory (ALCHEMI) Large Program. The dataset includes observations of the CO (1–0), (2–1), (3–2) and HCO^+ (1–0), (2–1), (3–2), (4–3) transitions. Integrated intensity (moment-0) maps were generated for each transition, and three representative regions of low, medium, and high brightness were selected for spectral extraction. We studied CO and HCO^+ to distinguish between neutral and ionic gas components.

By comparing the observed line intensities and CO/HCO^+ ratios with a grid of non-LTE radiative transfer models, we constrained the physical conditions of the gas across the different regions. We find that CO tends to trace lower-density gas (with $n_{H_2} \sim 2.78 \times 10^3$ cm^{-3} in all regions), while HCO^+ traces slightly denser and warmer gas, especially in the medium- and high-brightness regions (with n_{H_2} up to 7.74×10^3 cm^{-3} and T_{kin} reaching 283 K). The highest inferred abundance of HCO^+ (3.59×10^{-7}) is found in the low-emission region, though this may reflect modeling limitations or visual region selection biases. Our findings highlight how chemical and physical conditions vary across NGC 253's central molecular zone and underscore the need to account for optical depth effects and photoionization-driven chemistry in interpreting molecular line emission.

1. INTRODUCTION

1.1. *Interstellar Medium*

The interstellar medium (ISM) serves as both the site and the raw material for processes that play a central role in shaping galaxy evolution. While star formation is a primary outcome, the ISM is influenced by a wide range of physical mechanisms, including radiative interactions, thermal regulation, and active chemical pathways (Omont 2007). These physical conditions are encoded in the spectral lines emitted by atoms and molecules within the gas. As a result, molecular line observations offer powerful diagnostics of ISM properties, with different species serving as probes of distinct environmental conditions and energy sources (Martín et al. 2015). A broad and diverse molecular inventory is therefore necessary to fully characterize the physical and chemical processes taking place in such regions.

1.2. *NGC 253*

NGC 253, located at a distance of 3.5 ± 0.2 Mpc away (Rekola et al. 2005), is a nearby almost edge-on barred spiral galaxy in the Sculptor Group and is one of our closest examples of a nuclear starburst galaxy (Pence 1981). It is viewed nearly edge-on and exhibits a pronounced nuclear starburst, making it an ideal laboratory for studying the interplay between dense molecular gas and intense star formation (Puche et al. 1991). The galaxy's central molecular zone (CMZ), spanning approximately 300×100 pc, harbors a substantial reservoir of molecular gas on the order of $\sim 10^8\ M_\odot$ (Sakamoto et al. 2011). This accumulation of material is thought to result from gas inflow driven by a stellar bar, which extends roughly 2.5 kpc in deprojected length and is evident in the moment-0 maps. The rich interstellar medium (ISM) within the central kiloparsec is characterized by high gas densities, strong radiation fields, and complex chemistry, all of which are influenced by the ongoing starburst activity. This central region alone sustains a star formation rate of $\sim 2\ M_\odot\,\mathrm{yr}^{-1}$, contributing nearly half of the galaxy's total rate of 3.6–4.2 $M_\odot\,\mathrm{yr}^{-1}$ inferred from infrared luminosity measurements (Leroy et al. 2015). Since NGC 253 is undergoing a significant burst of star formation in its central region, it is an excellent target for studying the molecular gas properties that fuel such activity.

1.3. *Importance of HCO^+ and CO and this study*

In this study, we focus on two key molecular tracers: carbon monoxide (CO) and formylium (HCO^+). CO is the most abundant molecule after molecular hydrogen and serves as a classical tracer of cold, dense molecular gas, often used to infer total gas mass and large-scale structure. HCO^+, a molecular ion, is commonly used as a tracer of denser and more ionized regions within molecular clouds. Comparing the emission of CO and HCO^+ allows us to distinguish between neutral and ionized gas components, providing insight into the density structure, ionization state, and excitation conditions in the starburst nucleus.

Past studies of NGC 253 have focused on tracing dense gas through multiple molecular species, including HCN(1-0), HCO^+(1-0), and CO(1-0) (Knudsen et

[1] Department of Astronomy, University of Virginia, P.O. Box 3818, Charlottesville, VA 22903, USA
[2] NRAO, 520 Edgemont Rd, Charlottesville, VA 22903, USA

al. 2007). These investigations revealed that the central molecular zone of NGC 253 exhibits both elevated gas densities and chemical complexity, shaped by the ongoing starburst and potential outflows.

Our analysis leverages data from the ALCHEMI program which provides a full spectral scan of NGC 253's nucleus across ALMA Bands 3, 6, and 7 at $\sim 1''$ resolution. This unprecedented dataset allows for a uniform and detailed comparison of molecular tracers across multiple transitions and physical conditions. By comparing integrated intensities and line ratios of CO and HCO^+ transitions against non-LTE radiative transfer models, we aim to constrain the density, temperature, and ionization conditions within different regions of low, medium and high emission in the galaxy.

2. OBSERVATIONS

The ALMA data used in this analysis were obtained as part of the Cycle 5 Large Program `2017.1.00161.L`; for further information refer to Martín et al.(2017). The observations targeted the central molecular zone (CMZ) of NGC 253, centered at (J2000) $00^{\rm h}47^{\rm m}33.26^{\rm s}$, $-25°17'17.7''$, covering a rectangular field of $50'' \times 20''$ (850×340 pc) at a position angle of 65° east of north. The nominal angular resolution was $1''$ (17 pc), and the maximum recoverable scale was $15''$. The frequency coverage spans ALMA Bands 3 through 7, including a total of 47 tunings across the 84.2–373.2 GHz range, each consisting of four 1.875 GHz spectral windows from dual sidebands. A variable frequency overlap of 50–500 MHz within sidebands and 100–200 MHz between tunings ensured calibration consistency across the survey. The native spectral resolution was 0.977 MHz, corresponding to 3.4–0.8 km s^{-1} across the bands. Imaging was performed at a coarser, uniform velocity resolution. Primary beam corrections were applied to the data prior to analysis. Additional 12 m and 7 m array observations were included to achieve sensitivity to extended emission on spatial scales up to $15''$.

3. ANALYSIS

Spectral cubes were visualized and analyzed using *CARTA* (Cube Analysis and Rendering Tool for Astronomy), a software optimized for high-resolution three-dimensional data exploration. Each cube, composed of two spatial dimensions (x and y) and one spectral (frequency or velocity) axis, was used to study the spatial distribution of emission from various molecular transitions in NGC 253. To facilitate this, moment-0 maps were generated by integrating the flux along the frequency axis at each spatial pixel, resulting in two-dimensional images that represent the total intensity of emission over the full spectral line profile. This approach effectively captures the total energy emitted by a given transition at each position on the sky.

Moment-0 maps (Figures 1–7) were produced for each molecular transition under study, enabling both visual and quantitative assessments of the spatial distribution and intensity of molecular emission across the galaxy. From these maps, three representative regions of low, medium, and high brightness were selected (Figures 8–10). Each region was enclosed using a circular aperture with a diameter of $1.1354'' \times 1.2228''$, chosen to be smaller than or comparable to the synthesized beam size, thereby ensuring that each sample represents an independent spatial region within the galaxy. The brightness classification of each region was determined qualitatively based on visual inspection of the moment-0 maps. Regions were categorized as low-brightness if they appeared within more diffuse emission with no visible yellow intensities, medium-brightness if some moderate yellow intensities were present, and high-brightness if they coincided with areas of strong, concentrated yellow emission.

For each region, statistical measurements—including mean intensity, standard deviation, total flux density, and pixel count—were computed using *CARTA*. These observed values were then compared against model predictions from a radiative transfer grid using the chi squared(χ^2) statistic:

$$\chi^2 = \sum_i \frac{(O_i - M_i)^2}{\sigma_i^2} \tag{1}$$

where O_i is the observed intensity for transition i, M_i is the model-predicted intensity, and σ_i is the associated observational uncertainty (standard deviation). This statistic was computed across all observed transitions for each model in the grid, yielding a total chi-squared value per model that quantifies the overall goodness of fit. The O_i and σ_i values used for the χ^2 statistic are found in Tables 1-2.

TABLE 1
Observed Intensity and Standard Deviation for CO

	CO (1-0)	CO (2-1)	CO (3-2)
O_i(Low)	5.98×10^1	2.12×10^2	4.36×10^2
O_i(Medium)	1.08×10^2	4.14×10^2	8.23×10^2
O_i (High)	1.35×10^2	5.31×10^2	7.23×10^1
σ_i (Low)	3.32	1.26×10^1	3.20×10^1
σ_i(Medium)	7.79	3.79×10^1	1.33×10^2
σ_i (High)	1.64×10^1	4.06×10^1	1.69×10^2

TABLE 2
Observed Intensity and Standard Deviation for HCO^+

	HCO^+ (1-0)	HCO^+ (2-1)	HCO^+ (3-2)	HCO^+ (4-3)
O_i(Low)	6.44	1.81×10^1	1.57×10^1	1.35×10^1
O_i(Medium)	1.13×10^1	6.50×10^1	5.40×10^1	5.57×10^1
O_i(High)	2.68×10^1	8.99×10^1	9.40×10^1	1.30×10^2
σ_i(Low)	$4.20 \times 10-1$	1.52	2.11	2.19
σ_i(Medium)	1.08	9.41	9.08	1.02×10^1
σ_i(High)	3.93	1.14×10^1	1.64×10^1	2.50×10^1

To identify the most plausible physical conditions, the models were ranked by increasing χ^2, and the 100 best-fitting models (i.e., those with the lowest chi-squared values) were selected. By matching the indices of these models with the original radiative transfer grid, the corresponding physical parameters—such as density, temperature, H2 column density, and chemical abundance of CO and HCO^+ could be extracted. This enabled a quantitative comparison between observations and theoretical predictions, providing physical insight into the molecular gas conditions in NGC 253.

4. RESULTS AND DISCUSSION

We have found that parameters in the three different emission regions in the galaxy provide insight into the density, temperature, H_2 column density, and molecular abundance of the gas. By comparing the observed statistical measurements derived from the three representative regions with the outputs of the radiative transfer models, we were able to constrain key physical parameters of the molecular gas in NGC 253. Specifically, this comparison provides quantitative estimates of the gas volume density ($n_{\mathrm{H_2}}$), kinetic temperature (T_{kin}), molecular hydrogen column density ($N_{\mathrm{H_2}}$), and the chemical abundances of CO and HCO^+.

By isolating the 100 best-fitting models (lowest χ^2 values) for each region, we extracted the corresponding physical parameters and examined their distributions. These results are summarized in Tables 3–5, corresponding to the low-, medium-, and high-brightness regions, respectively. The comparison reveals how the physical conditions vary across different environments within the central molecular zone (CMZ) of NGC 253, and how the emission from CO and HCO^+ responds to changes in these conditions.

In the high-emission region, both CO and HCO^+ have similar derived densities on the order of 10^3–10^4 cm^{-3}, with HCO^+ slightly denser at 7.74×10^3 cm^{-3}. This density is lower than what is typically expected for HCO^+ in some environments, which may be explained by its nature as an ionic species. HCO^+ is often found in photoionized regions such as H II regions, where young, energetic stars create lower-density conditions via UV radiation. Since photoionization cannot penetrate dense columns of gas, the HCO^+ abundance observed here likely traces more diffuse, ionized material rather than the densest clumps. Interestingly, CO in this region may be optically thick, meaning that the observed emission only traces the surface layers of molecular clouds, masking emission from deeper layers. This saturation could explain why the CO density remains similar across different emission regions despite variations in brightness.

In the medium-emission region, the density of HCO^+ increases substantially compared to CO, further reinforcing the idea that HCO^+ traces slightly denser or differently illuminated gas. The temperature of HCO^+ also peaks here at 283 K—significantly higher than CO's 127 K—suggesting heating effects, possibly from nearby star formation or radiative feedback.

In the low-emission region, both molecular species show reduced temperatures and densities, but surprisingly, the HCO^+ abundance is higher than in the high-emission region. This counterintuitive result may be due to limitations in the modeling or the visual method used to select regions. It could also reflect chemical variations or stochastic effects in the lower-intensity areas. Therefore, this observation should be interpreted cautiously, and is likely not a physically meaningful trend but rather an artifact of analysis limitations.

4.1. *Limitations*

Several important limitations should be acknowledged:

- Region selection was performed manually based on visual inspection of moment-0 maps, which may introduce bias or variability in the derived parameters.
- Model limitations: We employed static, one-zone non-LTE radiative transfer models that do not account for complex dynamical or chemical processes, such as multi-phase gas structures or turbulence.
- No chemistry included: The modeling did not incorporate chemical networks or processes such as photoionization and photodissociation, which can have significant effects on species like HCO^+, especially in UV-rich environments. For instance, photoionization may enhance HCO^+ formation or alter its apparent abundance, depending on local UV flux.
- Optical depth effects: In the case of CO, optical thickness can saturate the emission line, leading to underestimates of column density and an inability to probe the full depth of molecular clouds.
- Parameter grid boundaries: In some cases, the best-fit abundances max out at the edge of the tested parameter space, particularly for HCO^+ in the high-emission region. This suggests that the true abundance may be even higher than inferred, and the lines could be optically thick or saturated.

TABLE 3
PARAMETERS FOR CO AND HCO^+ IN A LOW EMISSION REGION

	CO	HCO^+
Density (cm^{-3})	2.78×10^3	1.00×10^3
Temperature (K)	2.06×10^2	1.67×10^2
H_2 Column Density (cm^{-2})	4.64×10^{23}	4.64×10^{24}
Abundance	5.99×10^{-9}	3.59×10^{-7}

TABLE 4
PARAMETERS FOR CO AND HCO^+ IN A MEDIUM EMISSION REGION

	CO	HCO^+
Density (cm^{-3})	2.78×10^3	7.74×10^3
Temperature (K)	1.27×10^2	2.83×10^2
H_2 Column Density (cm^{-2})	4.64×10^{24}	4.64×10^{23}
Abundance	1.99×10^{-6}	5.99×10^{-9}

TABLE 5
PARAMETERS FOR CO AND HCO^+ IN A HIGH EMISSION REGION

	CO	HCO^+
Density (cm^{-3})	2.78×10^3	7.74×10^3
Temperature (K)	1.47×10^2	2.44×10^2
H_2 Column Density (cm^{-2})	4.64×10^{24}	4.64×10^{23}
Abundance	1.00×10^{-6}	1.67×10^{-8}

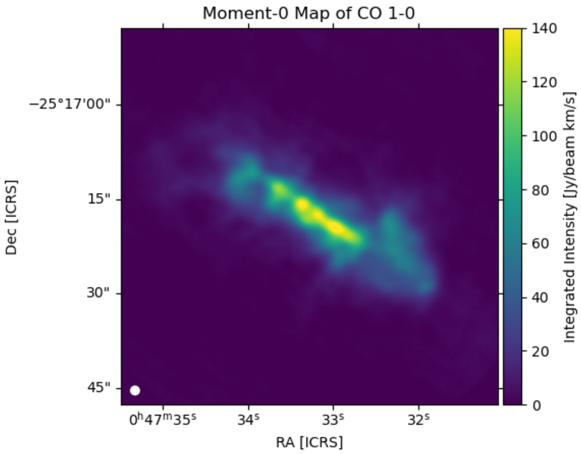

Fig. 1.— Moment-0 map of CO 1-0 transition. The synthesize beam is shown to the lower left.

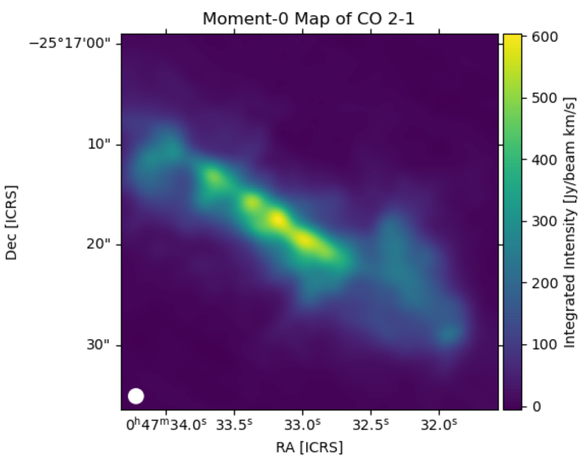

Fig. 2.— Moment-0 map of CO 2-1 transition. The synthesize beam is shown to the lower left.

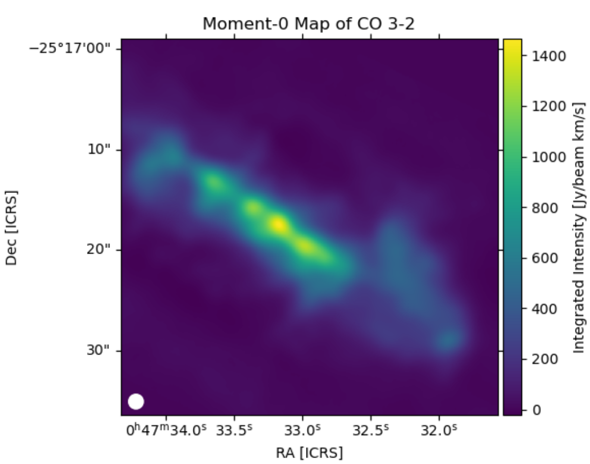

Fig. 3.— Moment-0 map of CO 3-2 transition. The synthesize beam is shown to the lower left.

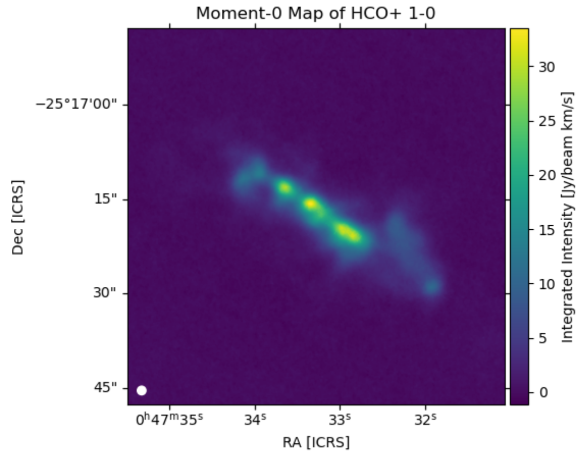

Fig. 4.— Moment-0 map of HCO+ 1-0 transition. The synthesize beam is shown to the lower left.

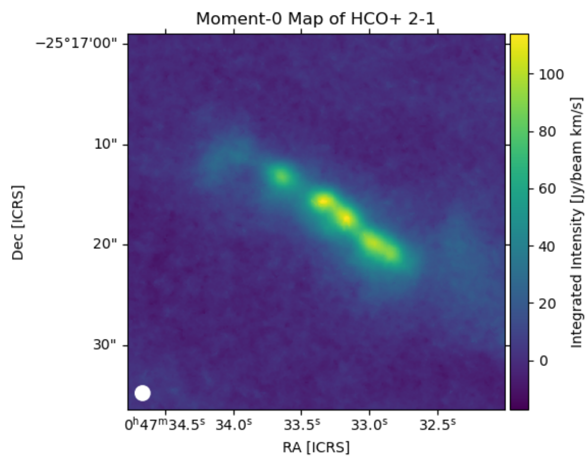

Fig. 5.— Moment-0 map of HCO+ 2-1 transition. The synthesize beam is shown to the lower left.

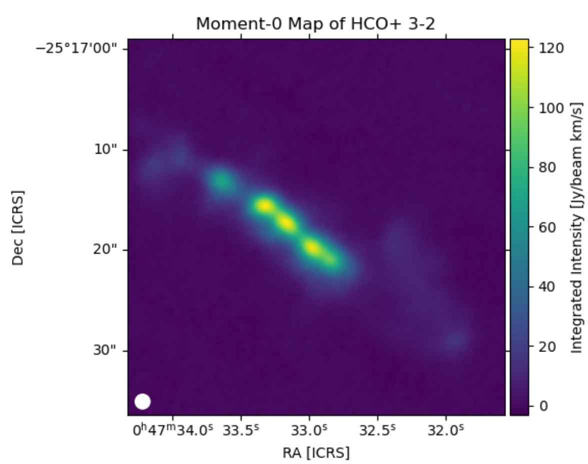

Fig. 6.— Moment-0 map of HCO+ 3-2 transition. The synthesize beam is shown to the lower left.

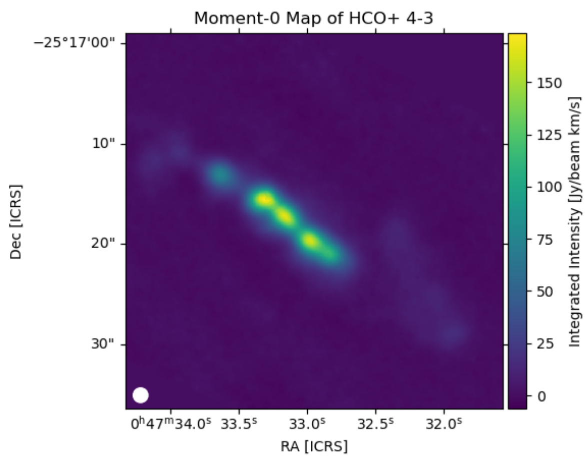

FIG. 7.— Moment-0 map of HCO+ 4-3 transition. The synthesize beam is shown to the lower left.

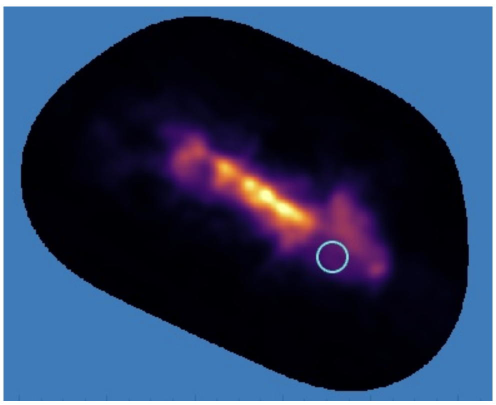

FIG. 8.— Circular aperture of size 1.1354287847" × 1.2227694598" styled in blue over an area deemed of low emission in moment-0 map of CO 2-1 transition.

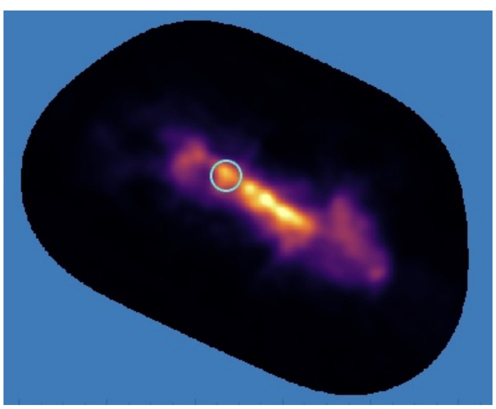

FIG. 9.— Circular aperture of size 1.1354287847" × 1.2227694598" styled in blue over an area deemed of medium emission in moment-0 map of CO 2-1 transition.

5. CONCLUSIONS

In this study, we have investigated the physical conditions and chemical properties of the molecular interstellar medium in the central region of NGC 253 using high-resolution ALMA observations of CO and HCO^+ across multiple rotational transitions. By constructing moment-0 maps and selecting representative regions of varying brightness, we performed a spatially resolved comparison between observational data and predictions from non-LTE radiative transfer models.

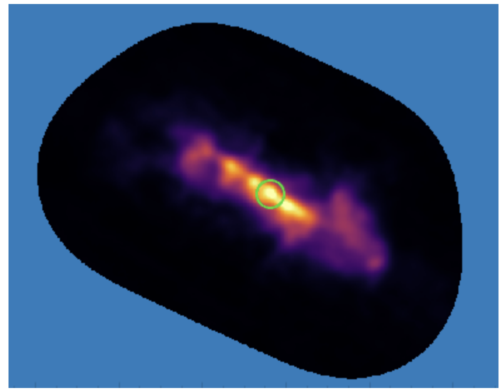

FIG. 10.— Circular aperture of size 1.1354287847" × 1.2227694598" styled in green over an area deemed of high emission in moment-0 map of CO 2-1 transition.

Our analysis reveals that CO emission is largely consistent across all three regions in terms of derived density ($n_{\mathrm{H}_2} \sim 2.78 \times 10^3$ cm^{-3}), suggesting possible optical thickness. In contrast, HCO^+ traces slightly denser and warmer gas, especially in the medium- and high-emission regions, where its density reaches 7.74×10^3 cm^{-3} and its temperature exceeds 240 K. Surprisingly, the highest inferred abundance of HCO^+ (3.59×10^{-7}) occurs in the low-emission region, a result that may reflect limitations in model fitting or region selection rather than physical reality.

These findings support the interpretation that CO primarily traces more diffuse, optically thick gas, while HCO^+ probes denser, more ionized environments—likely influenced by UV radiation from young stars. Additionally, the discrepancy in abundances between brightness regions suggests the presence of chemical and radiative processes not fully captured in our model grid.

5.1. *Future Work*

To address these limitations and better constrain the physical and chemical properties of the ISM in NGC 253, future studies could:

- Incorporate additional molecular tracers (e.g., HCN, CS, CO isotopologues) to probe a broader range of densities and environments.
- Include chemical modeling to capture the influence of photoionization, UV radiation, and molecular reactions.
- Utilize higher-resolution data to distinguish smaller-scale structures within the CMZ.
- Expand the parameter grid in radiative transfer modeling to avoid boundary effects in abundance or temperature fits.
- Analyze moment-1 and moment-2 maps to integrate kinematic and turbulent information into the interpretation of physical parameters.

6. ACKNOWLEDGMENTS

This work used ALMA data (ADS / JAO.ALMA 2017.1.00161.L). ALMA is a partner- ship of ESO (representing its member states), NSF (USA) and NINS (Japan), together with NRC (Canada) and NSC and ASIAA (Taiwan) and KASI (Republic of Korea), in cooperation with the Republic of Chile. The Joint ALMA Observatory is operated by ESO, AUI/NRAO and NAOJ.

7. REFERENCES

Leroy, A. K., Bolatto, A. D., Ostriker, E. C., et al. 2015, ApJ, 801, 25

Martín, S., Kohno, K., Izumi, T., et al. 2015, A&A, 573, A11

Omont, A. 2007, Reports on Progress in Physics, 70, 1099

Pence, W. D. 1981, ApJ, 247, 473

Puche, D., Carignan, C., & van Gorkom, J. H. 1991, AJ, 101, 456

Rekola, R., Richer, M. G., McCall, M. L., et al. 2005, MNRAS, 361, 330

Sakamoto, K., Mao, R.-Q., Matsushita, S., et al. 2011, ApJ, 735, 19